Composite Li-ion battery cathodes formed via integration of carbon nanotubes or graphene nanoplatelets into chemical preintercalation synthesis of bilayered vanadium oxides

Timofey Averianov, Ekaterina Pomerantseva

Department of Materials Science and Engineering, Drexel University, Philadelphia, Pennsylvania 19104, United States

Abstract

Bilayered vanadium oxides are attractive cathode materials for rechargeable batteries. The expanded interlayer space and versatile chemistries of these oxides yield high specific capacities. However, capacity retention and rate performance are limited due to structural instability and low electronic conductivity of these materials. Assembling the oxides with one- and two-dimensional carbon nanoparticles may produce highly efficient heterointerfaces that would enhance electrochemical charge storage properties. Here, we synthesize for the first time bilayered vanadium oxide composites with carbon nanotubes (CNTs) and graphene nanoplatelets (GNPs). The nanostructured carbons were initially functionalized by flash oxidation in air to create polar groups on the carbon surface and improve compatibility with aqueous chemical preintercalation synthesis route. Lithium preintercalated bilayered vanadium oxide, LVO (LVO = δ-$Li_xV_2O_5{\cdot}nH_2O$), was selected as a redox active oxide component to facilitate Li^+ ion diffusion through the interlayer region of δ-V_2O_5. A one-step process was developed to synthesize LVO/fCNT and LVO/fGNP composites by an *in situ* low temperature sol-gel method. We observed marked improvements in capacity retention and rate performance in the nanocomposites as compared to the pristine oxide, which were attributed to both improved electron transport and heterointerface stabilization effect enabled by integration with fCNTs and fGNPs. This work illustrates the ability to enhance material functionality through the *in situ* synthesis of nanocomposites with controllable heterointerface.

Keywords: bilayered vanadium oxide; carbon nanotubes; graphene nanoplatelets; nanocomposites; Li-ion batteries

Graphical Abstract

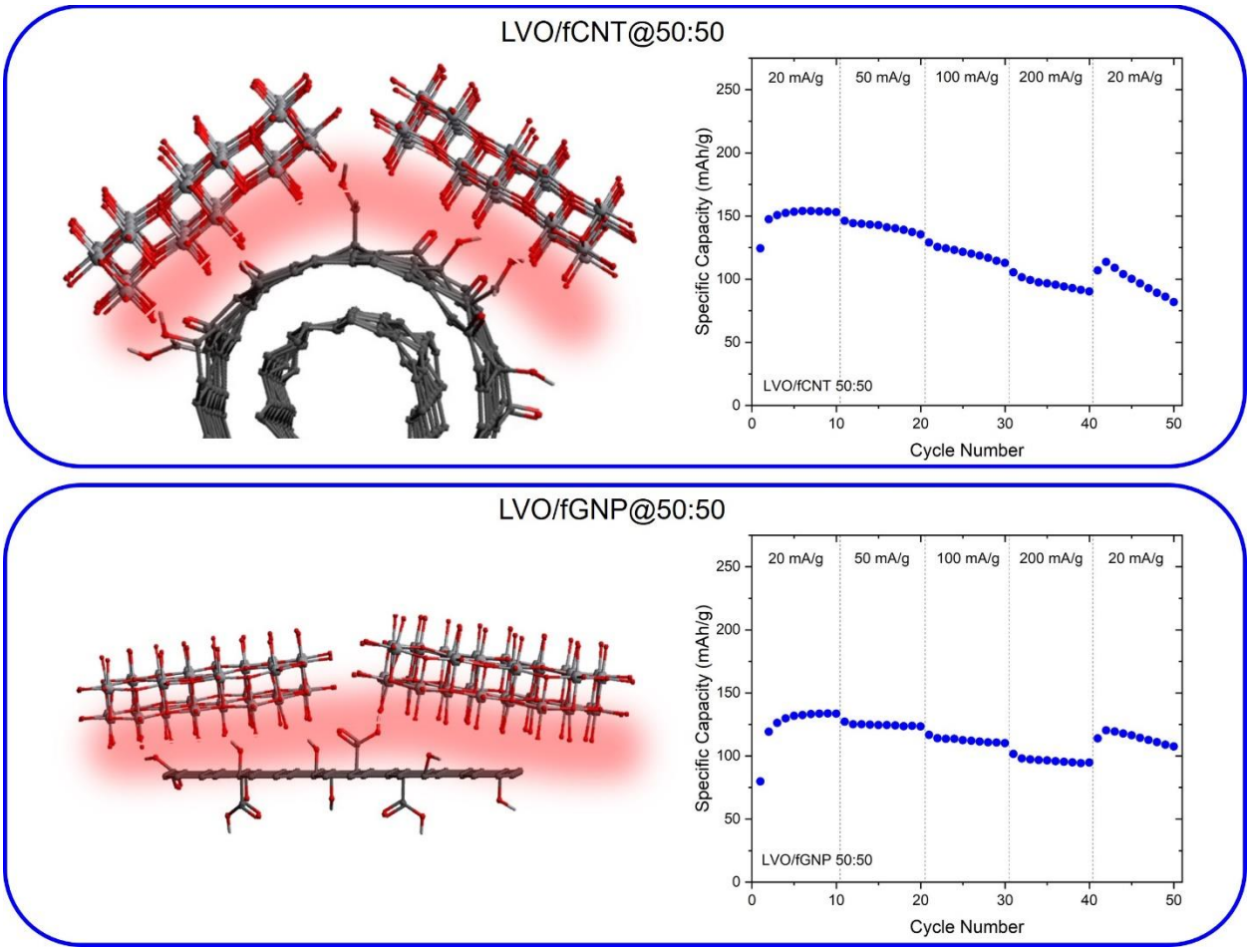

1. Introduction

Lithium-ion batteries have become a major success in reliable energy storage since their introduction in the 1990s. However, as batteries continue to phase out combustion-based energy sources, the components of the battery, in particular the electrodes, need to be iterated on to improve energy and power densities.[1] High power density in battery electrodes is typically indicated by fast ion diffusion coupled with rapid electron transport to facilitate the interaction of the mobile ion with the electrode structure. Transition metal oxides (TMOs) are the typical materials used for cathode production, due to their high working potential and capacities.[2] For high-power applications, fast ion diffusion needs to be matched with rapid electron transport. However, the electron transport in most oxides is limited due to the low electronic conductivity of these materials. In commercial cathodes, improved electronic conductivity is usually achieved by mixing active materials with conductive species to create electronic pathways in the electrode structure.[3-5] Among the most prominent examples of conductive additives are carbon nanomaterials. While carbon black has traditionally been used during electrode manufacturing, materials such as carbon nanotubes (CNTs) and graphene nanoplatelets (GNPs) have seen increased attention as additives due to their excellent electronic properties.[6, 7] The one-dimensional (1D) morphology of CNTs enables formation of highly conductive continuous networks through the assembly of individual nanotubes over a large area and thickness. The porosity of the produced networks can be varied providing pathways for electrolyte penetration. GNPs with two-dimensional (2D) morphology on the other hand offer their lateral surface for the growth of redox active material with the formation of a tight oxide/carbon contact combined with the excellent in-plane conductivity of graphene. In fact, via synthesis integration of active materials with CNTs and GNPs can lead to an intimate heterointerface with facilitated electron transport as compared to the physically mixed components. To synthesize homogeneous composite nanomaterials, both redox active and conductive components must be compatible with the synthesis medium to properly disperse at the nanoscale. Carbon nanomaterials are typically hydrophobic and agglomerate in aqueous syntheses leading to the absence of continuous electron conductive pathways. Functional groups like carboxyls and carbonyls can be grafted to the non-polar carbon surface to improve compatibility with water.[8, 9]

Layered transition-metal oxides have become a major driver in new materials for energy storage. Layered structures provide distinct pathways for ion diffusion that lead to higher and more consistent capacities than in materials with more dense, three-dimensional crystal structures. Vanadium oxides are a diverse family of layered TMOs that have been extensively studied in Li-ion battery systems.[10] The wide range of oxidation states of vanadium and versatile chemistry of vanadium oxides allow for the intercalation of multiple ions during synthesis and operation, leading to high capacities.[11-13] Bilayered vanadium

oxide, $\delta\text{-}V_2O_5 \cdot nH_2O$, is particularly attractive as a cathode material due to its vanadium chemistry and expanded interlayer region with a d-spacing of 11.5 Å which promotes ion diffusion and increases the number of intercalation sites.[14, 15] The versatility of the vanadium oxide chemistry allows for the pre-intercalation of not only inorganic ion of various size[15], but also organic molecules that can be carbonized to produce additional pathways for electron transport.[16]

Vanadium oxides have been used as components in nanocomposites along with CNTs and graphene for developing power-dense electrodes. Liu et al. have previously explored the integration of several vanadium oxides with reduced graphene oxides using hydrothermal methods, showing greater than 40% capacity retention exhibited by the composites up to a C-rate of $5C$ $(500\ mA/g)$.[17] Nanostructured honeycomb-like vanadium oxide/carbon nanotube networks showed overall capacity improvements as compared to vanadium oxide alone, with a remarkable 3x improvement of capacities at a current density of $1000\ mA/g$.[18] The incorporation of carbon nanomaterials appears to generally improve capacities and tolerance toward high currents as the carbon tends to equalize the electronic and ionic conductivity characteristics of the cathode material. However, *in situ* integration with carbon nanoparticles via synthesis has not been reported for bilayered vanadium oxides, which could provide another method for improving its electrochemical energy storage properties alongside post-synthesis treatments like hydrothermal treatment and annealing.[19, 20]

Here, we for the first time report the integration of bilayered vanadium oxide with CNTs and GNPs in two different mass ratios to demonstrate the effects of composition and morphology on rate capability of the produced nanocomposites in non-aqueous Li-ion cells. Lithium preintercalated bilayered vanadium oxide, LVO (LVO = $\delta\text{-}Li_xV_2O_5{\cdot}nH_2O$), was selected as a redox active oxide component to facilitate Li^+ ion diffusion through the interlayer region of $\delta\text{-}V_2O_5$.[21] 1D multi-walled CNTs and 2D GNPs were chosen to understand the role of conductive additive particles dimensionality. To enable compatibility with the aqueous chemical preintercalation synthesis approach, carbon nanoparticles were functionalized with the hydrophilic groups. This work furthers our synthetic capabilities for the preparation of multifunctional nanocomposites with enhanced conductivity and energy storage properties.

2. Experimental methods

Functionalization of carbon nanotubes and graphene nanoplatelets

Functionalized multi-walled carbon nanotubes (CNTs) and graphene nanoplatelets (GNPs) were prepared using a "flash oxidation" process adapted from Osswald et al.[9]. In brief, 1g of either the CNTs or GNPs was placed in a porcelain crucible and oxidized by oxygen in air at $550\ °C$ for 30 minutes before slowly cooling down to $25°C$ in a Thermo Scientific Lindberg Blue M programmable oven. Hereinafter, the flash-oxidized carbons are referred to as fCNTs and fGNPs, where the "f" stands for the presence of functional groups on the surface of the carbon after oxidation.[9]

Sol-gel synthesis of LVO/C nanocomposites

The LVO/C nanocomposites were prepared using an aqueous sol-gel synthesis adapted from Clites et al.[15], using an excess of lithium salt with a $Li{:}\,V$ ratio of 10:1. Two mass ratios of LVO to carbon were used to study the effects of composition on the generation of heterointerfaces and electrochemistry. Experimental values given here are for the LVO:C = 50:50 mass ratio, and the values used to prepare a composite with LVO:C = 70:30 mass ratio are provided in the **Supporting Information (Table S1)**. The nanocomposites are referred to using the type of carbon nanoparticle and the mass ratio, e.g., the LVO and fCNT nanocomposite synthesized with a 50:50 ratio is referred to as LVO/fCNT@50:50. $2.34\ g$ of LiCl (Fisher Scientific) were added to $15\ mL$ of deionized water in a glass beaker while stirring on a hot plate. $15\ mL$ of $30\ wt.\%\ H_2O_2$ solution (Fisher Scientific) and $0.5\ g$ of the functionalized carbon (either fCNTs or fGNPs) were then added to the solution while stirring, producing a dark grey suspension. $0.5\ g$ of α-V_2O_5 (98%, Fisher Scientific) was added slowly to the suspension over 20 minutes. The produced mixture was stirred for 1 hour at $25°C$. Then the temperature was raised to $60°C$, and stirring continued for another hour. After that $1\ mL$ of $30\ wt.\%\ H_2O_2$ solution was added to the mixture, which was further stirred for 2 more hours at $60°C$. The precipitate formed in a sol-gel process was aged for four days at room temperature. The aging step promotes the formation of the bilayered LVO phase. After aging, the samples were vacuum filtered, washed with deionized water, and dried at $105°C$ for 24 hours. The schematic of the synthesis process is shown in **Figure 1**. Notably, materials in this work were prepared without post sol-gel step hydrothermal treatment as our experiments indicated that hydrothermal treatment leads to the phase segregation with the formation of LVO and carbon clusters and broken conductive network connectivity (**Figure S1, Supporting Information**). For comparison, the pristine LVO phase was synthesized using the same procedure described above but without addition of fCNTs or fGNPs.

Materials Characterization

Structural analysis of the composite samples was performed using a Rigaku Miniflex 600 (Japan) powder X-ray diffractometer (XRD) with Cu Kα radiation. XRD patterns were collected using a step size of $0.02°$ and a step speed of $1° \ min^{-1}$. Morphological analysis of the samples was performed using a Zeiss SUPRA-50VP (Germany) scanning electron microscope (SEM) equipped with an Everhard-Thornley in-lens secondary electron detector. All images were taken at 3 keV and at a working distance of 5 mm. Compositional analysis was performed using TA Instruments Q50 thermogravimetric analyzer (TGA) by monitoring the mass of a sample during a temperature ramp up; the temperature range was $25°C$ to $1000°C$ and the heating rate was $10°C \ min^{-1}$. Degree of carbon functionalization was evaluated using a Renishaw inVia Raman microscope with a 514 nm Ar-ion laser. Raman spectra were collected from 100 to $2000 \ cm^{-1}$. Conductivity analysis was performed using a Jandel RM3000+ four-point probe test unit. Pellets for the conductivity measurements were prepared by loading $10 \ mg$ of powder into an $8 \ mm$ die and pressing the die at $60 \ kN$. The reported conductivity was determined via the following equation:

$$\sigma \ (S \ cm^{-1}) = \frac{1}{R_s \times t}$$

where R_s is the measured sheet resistance and t is the thickness of the pellet. To meet the requirement for the thickness of the pellet to be smaller than half of the probes distance (1 mm ± 10 μm), the pellets thickness was kept at 100-250 μm.

Electrode and Cell Fabrication

Electrodes were fabricated using an $80:10:10$ mass ratio of active material, activated carbon (YP50), and polyvinylidene fluoride (PVDF) (Kynar Flex, Alkema, USA), respectively. Activated carbon was used to enhance interparticle conductivity within the electrode film. The active material and activated carbon were hand ground in an agate mortar and pestle for 20 minutes and then further ground using zirconia milling media in a FlackTek DAC 150.1 FVK-K (USA) mixer. This mixture was then added to a solution of n-methyl-2-pyrrolidene (NMP) and PVDF and mixed until the suspension was homogeneous. The final slurry was then cast onto an aluminum foil current collector ($0.018 \ mm$, Fisher Scientific, USA) with a doctor blade set to $10 \ \mu m$. The cast electrode was set to dry at room temperature in a fume hood for 24 hours, after which electrode disks were prepared using a $12 \ mm$-diameter punch. The punched electrodes were set in an $105°C$ vacuum oven for 24 hours before being transferred to an argon-filled glovebox. The electrode disks were then used in the fabrication of 2032 coin cells. All coin cells were in a half-cell configuration, using lithium metal as the anode. A $25 \ \mu m$ trilayer polypropylene/polyethylene/polypropylene membrane (2325, Celgard, USA) was used as the separator.

LP40 (1 $M\ LiPF_6$ in 1:1 wt/wt ethylene carbonate (EC)/diethyl carbonate (DEC), Gotion, USA) was used as the electrolyte.

Electrochemical Characterization

All cells were tested within a potential range of $2.0 - 4.0\ V$ versus Li/Li^+. All potentials reported in this paper were measured with respect to a Li/Li^+ reference electrode. Cyclic voltammograms (CV) were obtained using a BioLogic VP3 potentiostat (France) at a sweep rate of $0.1\ mV\ s^{-1}$. Rate capability testing was performed using an Arbin battery testing station (LBT21084, USA) by cycling for 10 cycles at each of the following current densities: $20\ mA/g$, $50\ mA/g$, $100\ mA/g$, $200\ mA/g$, and then returning back to $20\ mA/g$. The full mass of nanocomposites, including the mass of CNTs and GNPs, was used as an active mass when calculating gravimetrically scaled values of current densities and specific capacities. Electrochemical impedance spectroscopy (EIS) Nyquist plots were obtained using a Gamry potentiostat in-line with the Arbin tester by applying a sine-wave signal across the cell. The frequency range for the signal was $0.01\ Hz - 200\ kHz$ at OCV, 0% SOC, and 100% SOC during the first cycle. SOC, or state of charge, is defined as a percentage of the upper and lower limits of the voltage window, i.e., 0% SOC corresponds to $2\ V$ versus Li/Li^+, and 100% SOC corresponds to $4\ V$ versus Li/Li^+.

3. Results and discussion

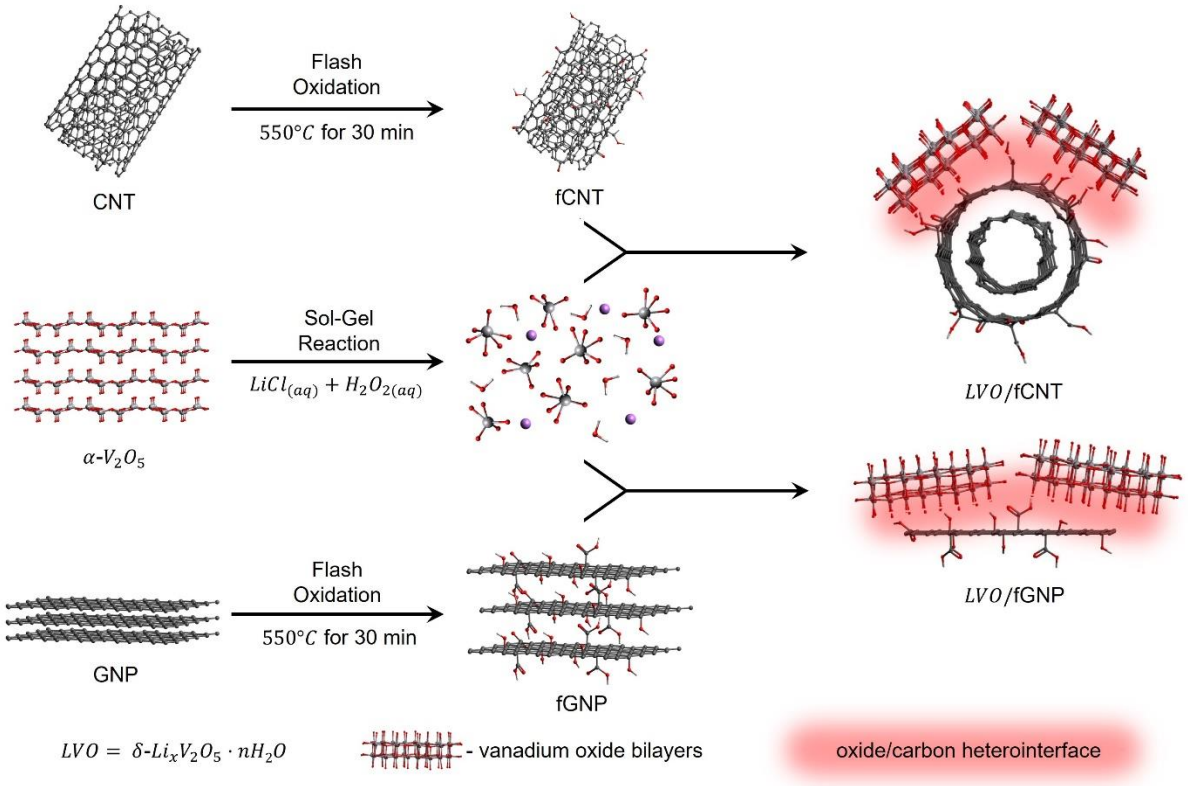

Figure 1. Schematic illustration of the synthesis approach for the preparation of LVO/fCNT and LVO/fGNP nanocomposites.

The degree of CNTs and GNPs functionalization was evaluated using Raman spectroscopy. The Raman spectra for both of the as-received and functionalized carbons are shown in **Figure 2**. The characteristic feature in Raman spectra for determining the degree of functionalization in sp^2-hybridized carbon materials is the ratio of intensities of the D-band and the G-band (I_D/I_G). The G-band corresponds to the stretching mode of $C-C$ bonds and is a measure of the relative density of sp^2 carbons present.[22] The D-band corresponds to disorder in the structure due to defects introduced in the carbon lattice. The introduction of functional groups on the surface of the carbon acts as defects which is reflected in the Raman spectra as an increase in the D-band intensity.[22] **Figure 2** shows that the I_D/I_G ratio increased after the carbons were flash-oxidized. The oxidation of the CNTs showed an I_D/I_G increase from 1.072 to 1.180, and in case of the GNPs an increase from 0.0457 to 0.213. The effects of oxidation were also observable in the change in electronic conductivity, listed in **Table S2** (**Supporting Information**). The reduction in the overall sp^2 carbon content after functionalization reduces the available pathways for fast electron transport, decreasing carbon conductivity.

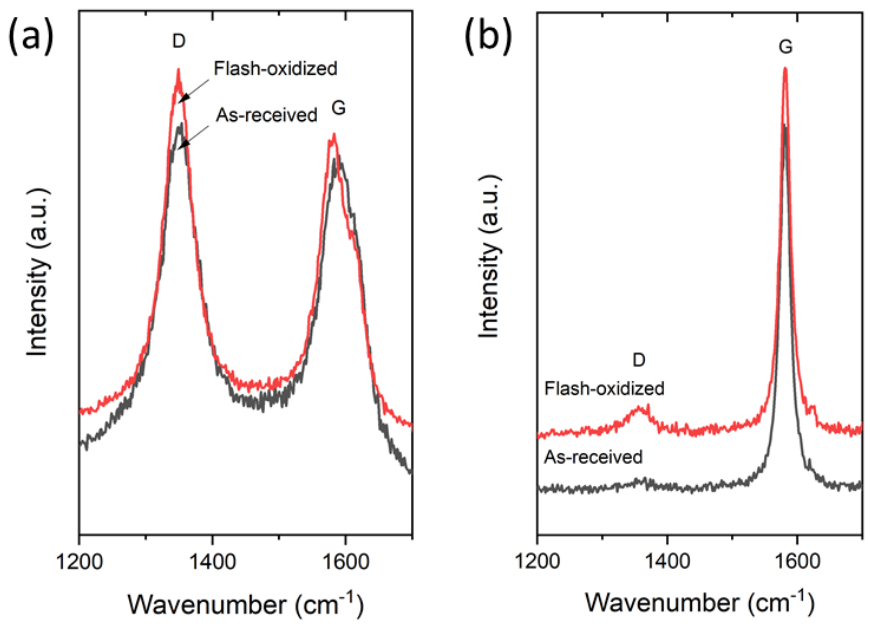

Figure 2. Raman spectra of the as-received (black line) and flash-oxidized (red line) (a) multiwalled carbon nanotubes and (b) graphene nanoplatelets.

SEM images of the LVO/C nanocomposites are shown in **Figure 3**. Both LVO/fCNTs and LVP/fGNPs composites are visually homogenous (low magnification images in **Figure 3a, 3c, 3e and 3g**). However, the morphology of each composite depends on the geometry of carbon nanoparticles used. Because of the relatively small diameter and high aspect ratio of the functionalized carbon nanotubes, the vanadium oxide grows around and in the pores of the CNTs-formed framework and envelops the nanotubes. (**Figure 3**, **a-b** and **e-f**). The resulting structure resembles fiber reinforcement of polymers, where fCNTs play a role of the reinforcing fibers. In contrast, the large lateral size of the functionalized graphene nanoplatelets allows the LVO sheets to grow on top of the fGNPs, similar to laminate composites (**Figure 3**, **c-d** and **g-h**). As a result, the oxide/carbon contact area, or heterointerface, is maximized in case of LVO/GNPs nanocomposites compared to the LVO/fCNTs structures.

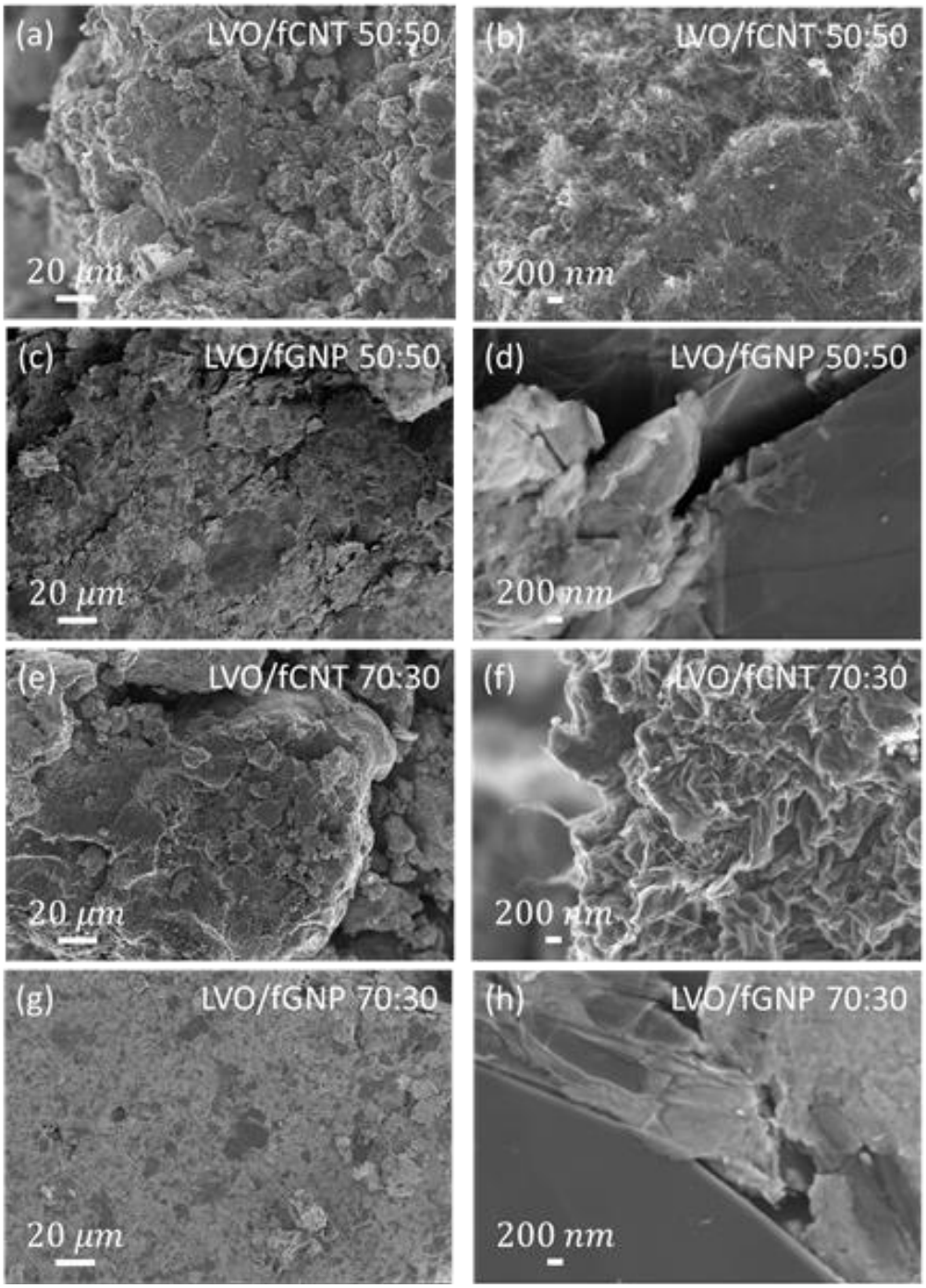

Figure 3. SEM images of the LVO/carbon nanocomposites; (a, b) LVO/fCNT with 50:50 weight ratio,(c, d) LVO/fGNP with 50:50 weight ratio, (e, f) LVO/fCNT with 70:30 weight ratio, and (g, h) LVO/fGNP with 70:30 weight ratio.(a, c, e, g) Low- and (b, d, f, h) high-magnification images are shown.

The phase composition of the synthesized nanocomposites was investigated via XRD measurements. The XRD patterns of the LVO/fCNT and LVO/fGNP nanocomposites are shown in **Figure 4a** and **Figure 4b**, respectively. For comparison, the diffraction patterns of the individual components, pristine LVO and carbon nanoparticles, are provided. There are two main reflections in the XRD patterns of all four materials: a broad peak between $7 - 7.5°$ 2θ and a peak at $\sim 26°$ 2θ that is broad for the fCNT composites and narrow for the fGNP composites. The peak between $7 - 7.5°$ 2θ corresponds to the (001) reflection, from which the d-spacing of the LVO phase can be calculated [21]. The peak shift observed when comparing XRD patterns of the pristine LVO phase and LVO/C nanocomposites is most likely related to the formation of a heterointerface between the LVO and the carbon components. The d-spacing for the LVO/fCNT composites was calculated to be 11.730 Å for the 50:50 sample and 12.864 Å for the 70:30 sample; for the LVO/fGNP composites, the d-spacing was calculated to be 12.162 Å for the 50:50 sample and 12.837 Å for the 70:30 sample. The variance in d-spacings between the samples obtained using different LVO:C weight ratios indicates that the d-spacing of the nanocomposite can be tuned by changing the composition of the composite, but only a specific composition will yield a maximum possible spacing. A wider interlayer region could enable increased capacities by improving diffusion-limited processes, affecting both redox and capacitive behaviors [23]. The peak around $26°$ 2θ corresponds to two overlapping features: the (003) plane of the LVO and the carbon d-spacing [24, 25]. In the XRD patterns of LVO/fCNT composites, this peak is similarly broad as the peak in the XRD pattern of fCNTs, and the intensity of this reflection is directly related to the amount of carbon present in the composite. The XRD patterns of LVO/fGNP composites show similar behavior, however the peaks corresponding to the carbon d-spacing are narrower than the carbon d-spacing peaks in the LVO/fCNT composites. The fGNPs' layers are more compact than the fCNTs' concentric tubes, which narrows the d-spacing distribution. The analysis of the XRD patterns of the synthesized LVO/carbon nanocomposites clearly indicates that the presence of either fCNTs or fGNPs in the reaction mixture affects the crystallization process of chemically prelithiated bilayered vanadium oxide and leads to the modification of the LVO structure. The latter, however, cannot be easily understood from the XRD patterns and rather requires a more detailed structure analysis, such as structure refinement using pair distribution function (PDF) approach.[14] PDF data analysis can explain the evolution of the XRD patterns in the presence of a certain type of carbon nanostructures during chemical preintercalation synthesis, however, it is outside of the scope of this work and requires a separate study.

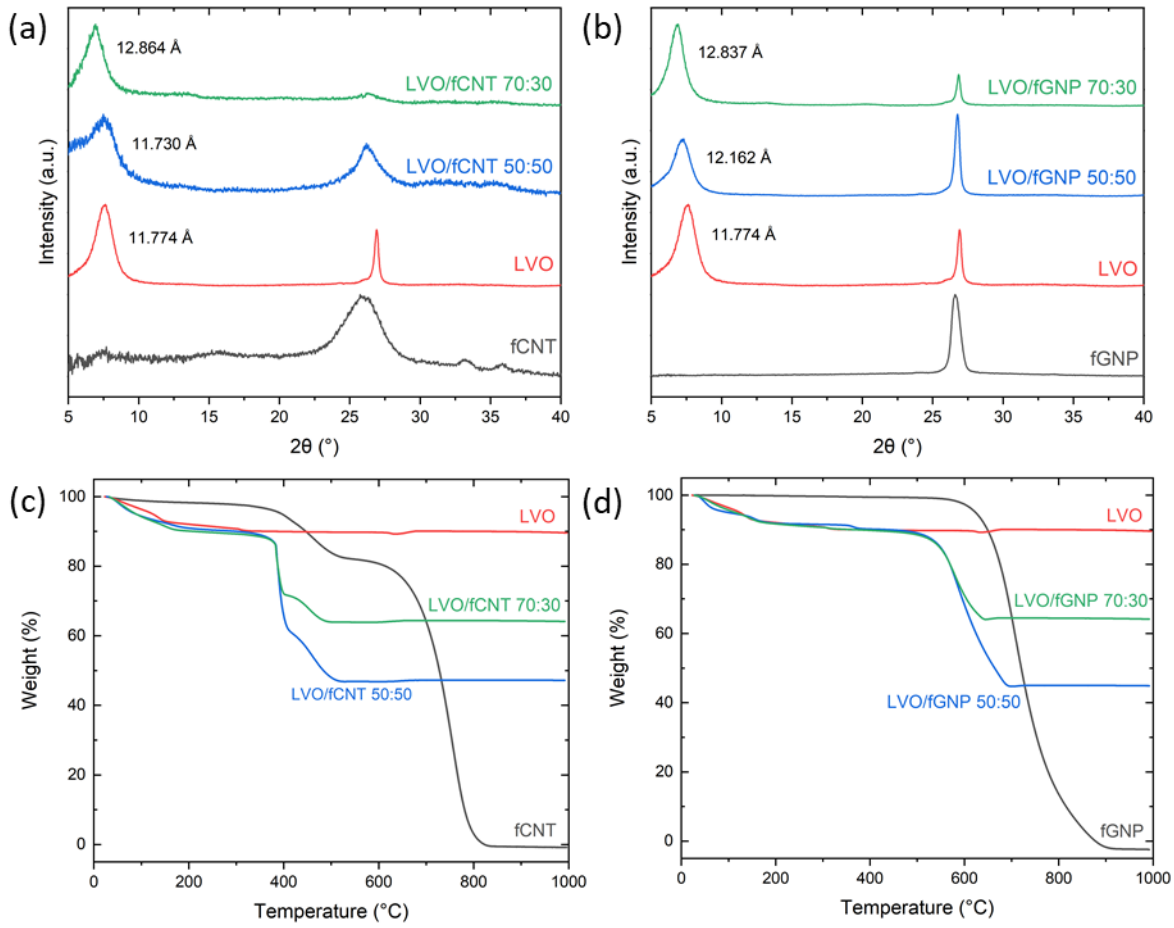

Figure 4. (a,b) XRD patterns of the (a) fCNT- and (b) fGNP-based LVO nanocomposites in comparison to the XRD patterns of individual materials. (c,d) TGA weight loss curves for (c) LVO/fCNT and (d) LVO/fGNP nanocomposites.

The composition of the LVO/carbon nanocomposites was confirmed via thermogravimetric analysis (TGA). The TGA weight loss curves for the LVO/fCNT and LVO/fGNP nanocomposites are shown in **Figure 4c** and **Figure 4d**. The composite components react in two distinct ways upon heating to $1000\,°C$ in air: the LVO shows a net weight loss of about 10%, while the nanocarbons are completely oxidized to CO and CO_2 gases, leading to the complete evaporation of the carbon above $900°C$. Based on these behaviors, the composition can be determined by observing the weight loss of the composite past a given temperature. Surprisingly, the temperature at which major carbon evaporation occurs varies on the carbon used. fCNTs show a two-step oxidation process, an initial oxidation at $400°C$ and a complete evaporation at $600°C$ whereas the fGNPs only show one step, evaporation at $600°C$. The two-step oxidation of the fCNTs is in agreement with previous studies, but the fGNPs show high thermal stability as compared to other graphene oxides and reduced graphene oxides.[26, 27] The lower temperature of carbon evaporation in case of nanocomposites as compared to individual carbons can be attributed to the oxidizing

nature of vanadium oxide present in a tight contact with carbon. As a result, oxygen atoms from the oxide structure can promote oxidizing reactions with carbon leading to the lower temperatures observed in TGA weight loss curves (**Figure 4, c-d**). Measuring the weight loss after these temperatures can be used to evaluate the carbon content in the nanocomposites. The LVO/fCNT@50:50 and LVO/fGNP@50:50 showed a weight loss of 44.1% and 47.0%, respectively, after the onset of carbon oxidation/evaporation; the LVO/fCNT@70:30 and LVO/fGNP@70:30 showed a loss of 26.0% and 27.5%, respectively.

Four-point probe conductivity measurements were performed to evaluate the in-plane conductivity of each composite sample and understand the role of carbon addition in electronic conductivity of LVO. The measured thicknesses, t, of the pellets and the calculated conductivities, σ, are listed in **Table 1**. The measured conductivities confirm that the addition of the carbon increased the in-plane conductivity of the LVO, in this case by 3-4 orders of magnitude. The conductivities also scaled with the amount of carbon in each sample such that greater amounts of carbon yielded higher conductivity values. Additionally, the LVO/fGNP nanocomposites showed more than twice the conductivity of the LVO/fCNT composites, which can be attributed to the differences in conductivities of the carbon component in the composite. From four-point probe measurements, the fGNP exhibited 2 orders of magnitude greater conductivity to the fCNT (**Table S2, Supporting Information**). The low electronic conductivity of the fCNT ($3.52\ S/m$) is likely a factor of the measurement method. The pressed fCNT pellet has nanotubes randomly oriented and the point-to-point contacts of the one-dimensional particles create a nonuniform distribution of electronic pathway lengths.

Table 1. Average thickness (t) and electronic conductivities (σ) of the pressed pellets made of powders with the composition shown in the first column. Values in parenthesis are the standard errors of the mean for three measurements.

Material	$t,\ \mu m$	$\sigma,\ S\ cm^{-1}$
LVO	$203.33(\pm 1.67)$	$0.00529(\pm 0.001)$
LVO/fCNT@50:50	$163.33(\pm 0.33)$	$11.97(\pm 0.50)$
LVO/fCNT@70:30	$172.67(\pm 1.33)$	$4.08(\pm 0.14)$
LVO/fGNP@50:50	$103.67(\pm 1.33)$	$28.35(\pm 2.76)$
LVO/fGNP@70:30	$139.33(\pm 0.33)$	$8.48(\pm 0.42)$

The electrochemical performance of the LVO/carbon nanocomposites was evaluated in Li-ion half-cells. To understand the effects of the CNTs and GNPs integration, reference cells containing pristine LVO electrodes were cycled. **Figure 5** shows the cyclic voltammograms of the Li-ion cells containing nanocomposite electrodes. The composites showed a significant improvement in stability over the reference LVO electrodes (**Figure S2** in **Supporting Information**). **Figure 5** shows that similar intercalation peaks can be observed on the first reduction and oxidation steps in the nanocomposite and reference electrodes ($2.47\,V$ and $2.84\,V$ on reduction, $2.60\,V$ and $2.91\,V$ on oxidation), but the peaks are substantially more defined in case of the cells with composite materials. For instance, when comparing specific currents for the $2.60\,V$ peak on oxidation between the $LVO/fCNT$@50:50 and the reference electrodes, the composite electrode output a maximum specific current of $73.1\ mA/g$ while the same peak for the reference electrode only displayed a current of $9.3\ mA/g$. The reference electrode also begins to degrade immediately on the first oxidation step, with the formation of an additional anodic peak at $3.75\,V$ that shifts to lower potentials with each subsequent cycle. The fast degradation of the LVO electrode is attributed to the synthesis method used in this work. In fact, to avoid phase segregation and disintegration of the heterointerface we excluded hydrothermal treatment synthesis step known to improve both specific capacity and electrochemical stability of the chemically preintercalated bilayered vanadium oxides [19]. Additionally, in this work we have not optimized the electrode drying conditions. As a result, the interlayer water content in a reference LVO electrode can be high, leading to poor stability. Low-temperature vacuum annealing could potentially be used to further improve electrochemical performance of the bilayered vanadium oxide electrodes.[20] However, this work is focused on understanding the role of CNTs and GNPs integration, and conclusions can be made as long as the synthesis conditions are kept the same for all materials studied in this work. The CV curves of the cells containing nanocomposite electrodes revealed excellent 5-cycle stability (**Figure 5**). The improved stability can be related to improved crystallinity of the LVO phase due to the growth on carbon surfaces.

The voltammograms of the Li-ion cells containing nanocomposites with different LVO:carbon ratios support the suggestion that there is an optimal ratio of bilayered vanadium oxide to carbon that would promote the highest capacity while maintaining stability over multiple cycles. The composites with a 70:30 mass ratio exhibited higher maximum capacities than those with 50:50 ratio, which is attributed to the larger amount of the redox active LVO phase in the nanocomposite structure (**Figure S3** in **Supporting Information** and **Figure 6**).

Of note is the behavior of the anodic peaks. The CV curves of the cells containing 50:50 nanocomposites showed three anodic peaks (**Figure 5, a-b**). However, in case of the cells containing 70:30 nanocomposites, the anodic peak at 2.60 V disappeared and the 2.71 V anodic peak became the dominant

feature (**Figure 5, c-d**), implying that the mechanism of charge storage could change dependent on the LVO-to-carbon ratio in the nanocomposites structure. Additionally, even after cycling for five intercalation/extraction cycles the differences in electrochemical stability are noticeable. As the amount of the redox active LVO phase in the nanocomposites structure increased, the capacity decay was more pronounced (**Figure 5** and **Figure 6**). This observation suggests that CNTs and GNPs presence in the reaction mixture during synthesis affects crystallization of the redox active phase. As the amount of LVO increased, the effect of carbon presence was less pronounced leading to the poorer electrochemical stability.

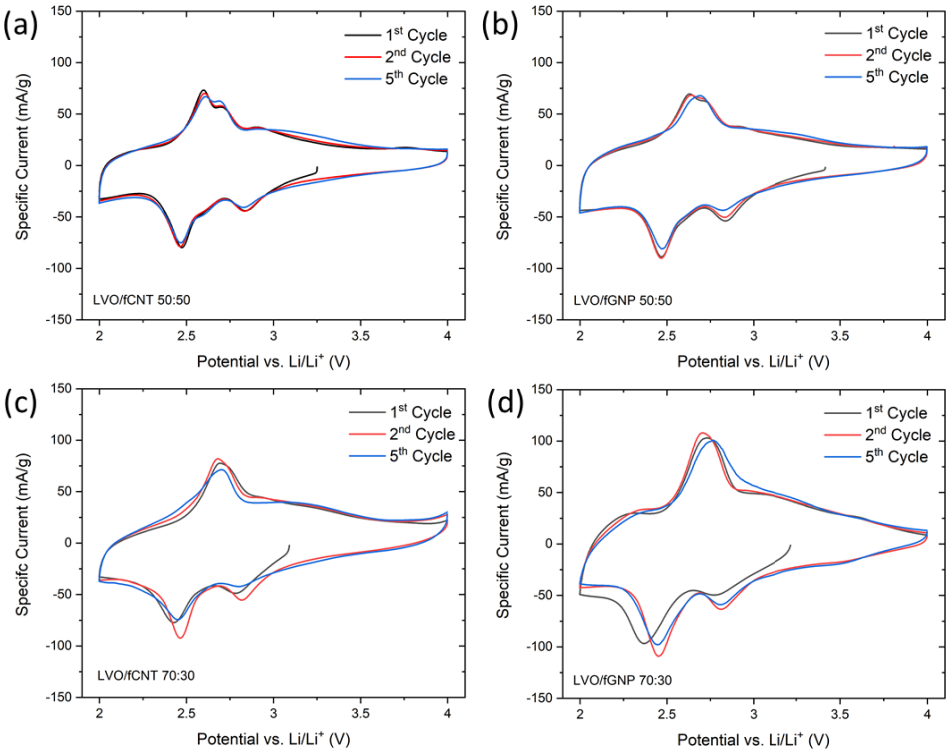

Figure 5. Cyclic voltammograms of the (a,c) fCNT-based composites and (b,d) fGNP-based composites. Voltammograms were collected at a scan rate of 0.1 mV/s.

Because the amount of carbon in the 70:30 composites is comparable to the amount of carbon black that is typically added in the process of conventional electrode fabrication, we evaluated electrochemical charge storage properties of the LVO/fGNP@70:30 electrode made without carbon black addition (**Figure S4** in **Supporting Information**). The performance for this electrode was significantly worse even compared to the reference LVO cell (**Figure S2, Supporting Information**), with a lower initial capacity and more rapid capacity fade. These results are indicative of the importance of the interparticle pathways for the electron transport, which are created through the addition of carbon black. Without carbon black, the particle-to-particle contact is poor, which hampers the conduction of electrons through the electrode microstructure. In the case of the composite electrodes with carbon black present, the nanocarbons are most

likely providing improved electron transfer within the composite oxide/carbon particle. However, an interparticle additive is still necessary to connect the particles together for the appropriate electronic conductivity at the electrode scale.

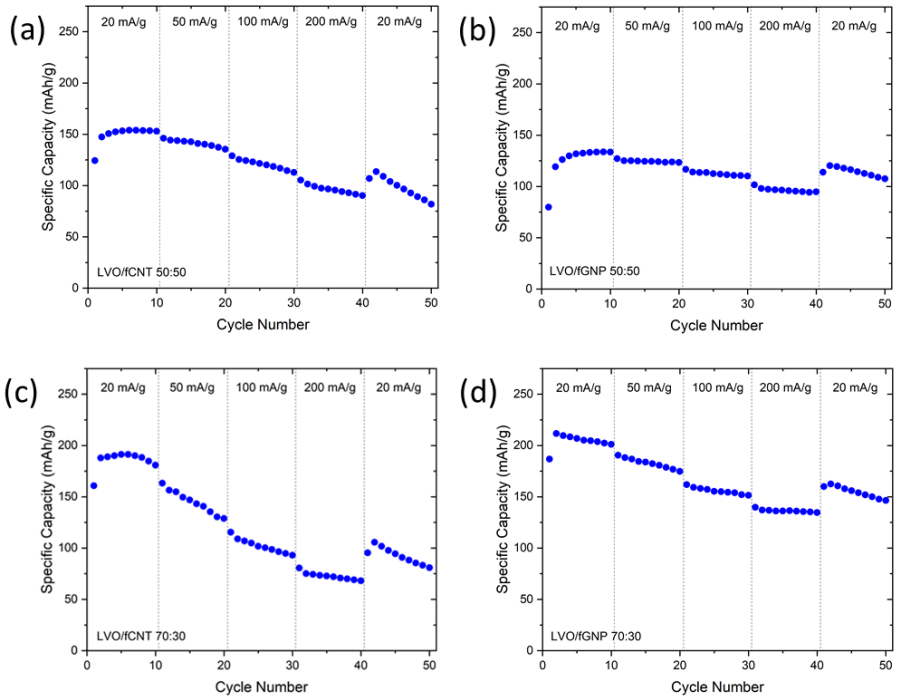

Figure 6. Rate performance of the LVO/carbon nanocomposites: (a) LVO/fCNTs with the weight ratio of 50:50, b) LVO/fGNPs with the weight ratio of 50:50, c) LVO/fCNTs with the weight ratio of 70:30, d) LVO/fGNPs with the weight ratio of 70:30. The following current densities, also shown in each panel, were used in the experiment: 20 mA/g, 50 mA/g, 100 mA/g, 200 mA/g, and then back to 20 mA/g.

The rate performance of the LVO/fCNT and LVO/fGNP nanocomposite electrodes is shown in **Figure 6**. In all cells, the first cycle capacity is lower than the maximum capacity attained in subsequent cycles. The 1st-to-2nd cycle capacity increase can be attributed to the presence of lithium ion in the interlayer region of pristine LVO phase. Chemically preintercalated Li^+ ions are extracted on the first charge cycle thus freeing additional space for the subsequent intercalation during the 2nd discharge cycle compared to the 1st discharge cycle. This effect is also visible in the next few cycles for the 50:50 composite electrodes and the $fCNT$-based 70:30 electrode, although to not as great of an extent as at the 1st-to-2nd cycle.

The tolerance to high currents is evaluated by comparing the drops in specific discharge capacity with increasing current densities. Comparison of LVO/fCNT and LVO/fGNP nanocomposite electrodes with different LVO-to-carbon ratios revealed several trends. First, the specific capacity of the @50:50 nanocomposites was found to decay more slowly than that of the @70:30 nanocomposites during cycling at increasing current densities (**Figure 6**). In fact, capacity of 68.07 mAh/g was exhibited by the

LVO/fCNT@70:30 electrode after 10 cycles at a current density of 200 mA/g, which is 35.60% of the maximum capacity shown by this electrode in the rate capability experiment (**Figure 6c**). At the same time, the LVO/fCNT@50:50 nanocomposite demonstrated 58.70% capacity retention (90.33 mAh/g at 10^{th} discharge cycle at 200 mA/g vs 153.88 mAh/g maximum capacity at 20 mA/g) (**Figure 6a**). Similar trends were observed for the LVO/fGNP nanocomposites. LVO/fGNP@70:30 showed 60.76% capacity retention (134.68 mAh/g at 10^{th} discharge cycle at 200 mA/g vs 211.66 mAh/g maximum capacity at 20 mA/g) and LVO/fGNP@50:50 showed 70.58% capacity retention (94.29 mAh/g at 10^{th} discharge cycle at 200 mA/g vs 133.59 mAh/g maximum capacity at 20 mA/g) under the same experimental conditions (**Figure 6b, d**). This result is attributed to the less pronounced heterointerface stabilization effect as the amount of the redox active LVO phase in the nanocomposite structure increases. Second, at the fixed electrode composition, LVO nanocomposites synthesized with fGNPs showed better electrochemical stability compared to the LVO/fCNT materials. This observation highlights the role of the nanostructured carbon dimensionality. The large flat lateral surface area of graphene nanoplatelets appears to be a better substrate for the LVO growth than the curved surface of CNTs. The more pronounced GNP stabilization effect may arise from the compatibility of the layered crystal structures of the oxide and graphene phases. All nanocomposites demonstrated substantially enhanced rate capability compared to the reference LVO electrode (**Figure S2b, Supporting Information**), which is attributed to both improved electron transport and heterointerface stabilization effect enabled by integration with CNTs and GNPs.

4. Conclusions

Bilayered vanadium oxide-based nanocomposites containing δ-$Li_xV_2O_5{\cdot}nH_2O$ (LVO) with carbon nanotubes (CNTs) or graphene nanoplatelets (GNPs) with the LVO:carbon weight ratios of 50:50 and 70:30 were for the first time synthesized by introduction of the carbon nanoparticles into chemical preintercalation synthesis process. Oxide/carbon integration with homogeneous distribution of two components became possible due to carbon functionalization via flash oxidation, which improved compatibility of CNTs and GNPs with aqueous synthesis route via surface functionalization leading to better hydrophilicity. Nanocomposite electrodes outperformed pristine LVO electrode when cycled in Li-ion cells. Improved rate capability was attributed to the increased electronic conductivity due to the integration with CNTs and GNPs. The superior capacity retention could be due to the oxide/carbon heterointerface stabilization effect. The stabilization effect was more pronounced in case of LVO nanocomposites with GNPs most likely due to the planar lateral surface enabling more efficient integration with the oxide phase growing from solution during synthesis. Our work demonstrates the potential of oxide/carbon heterointerface to not only improve

charge storage properties of intercalation cathodes but also aid in development of synthetic strategies leading to multifunctional materials with advanced properties.

Acknowledgements

This work was supported by the National Science Foundation Grant Nos. DMR-1752623 and DMR-1609272. We acknowledge Drexel's Centralized Research Facilities for help with materials characterization.

Author Information

Corresponding Author:

Phone: 215-571-4612; Email: ep423@drexel.edu

Author Contributions

E.P. developed the concept and designed the experiments. T.A. carried out experimental work including synthesis, characterization, and electrochemical testing. Both authors contributed to the analysis and interpretation of the obtained experimental data and writing of this manuscript.

References

1. Manthiram, A., *An Outlook on Lithium Ion Battery Technology.* ACS Central Science, 2017. **3**(10): p. 1063-1069.
2. Nitta, N., F.X. Wu, J.T. Lee, and G. Yushin, *Li-ion battery materials: present and future.* Materials Today, 2015. **18**(5): p. 252-264.
3. Amin, R. and Y.-M. Chiang, *Characterization of Electronic and Ionic Transport in $Li_{1-x}Ni_{0.33}Mn_{0.33}Co_{0.33}O_2$(NMC333) and $Li_{1-x}Ni_{0.50}Mn_{0.20}Co_{0.30}O_2$(NMC523) as a Function of Li Content.* Journal of The Electrochemical Society, 2016. **163**(8): p. A1512-A1517.
4. Amin, R., D.B. Ravnsbæk, and Y.-M. Chiang, *Characterization of Electronic and Ionic Transport in $Li_{1-x}Ni_{0.8}Co_{0.15}Al_{0.05}O_2$(NCA).* Journal of The Electrochemical Society, 2015. **162**(7): p. A1163-A1169.
5. Pomerantseva, E. and Y. Gogotsi, *Two-dimensional heterostructures for energy storage.* Nature Energy, 2017. **2**(7).
6. Presser, V. and Y. Gogotsi, *Carbon Nanomaterials First Edition*. Carbon Nanomaterials, 1st Edition, ed. Y. Gogotsi and V. Presser. 2006, Boca Raton: Crc Press-Taylor & Francis Group.
7. Presser, V. and Y. Gogotsi, *Carbon Nanomaterials Second Edition*. Carbon Nanomaterials, 2nd Edition, ed. Y. Gogotsi and V. Presser. 2014, Boca Raton: Crc Press-Taylor & Francis Group.
8. Paloniemi, H., T. Ääritalo, T. Laiho, H. Liuke, N. Kocharova, K. Haapakka, F. Terzi, R. Seeber, and J. Lukkari, *Water-Soluble Full-Length Single-Wall Carbon Nanotube Polyelectrolytes:*

Preparation and Characterization. The Journal of Physical Chemistry B, 2005. **109**(18): p. 8634-8642.
9. Osswald, S., M. Havel, and Y. Gogotsi, *Monitoring oxidation of multiwalled carbon nanotubes by Raman spectroscopy.* Journal of Raman Spectroscopy, 2007. **38**(6): p. 728-736.
10. De Jesus, L.R., J.L. Andrews, A. Parija, and S. Banerjee, *Defining Diffusion Pathways in Intercalation Cathode Materials: Some Lessons from V_2O_5 on Directing Cation Traffic.* ACS Energy Letters, 2018. **3**(4): p. 915-931.
11. Livage, J., *Sol-gel chemistry and electrochemical properties of vanadium oxide gels.* Solid State Ionics, 1996. **86-88**: p. 935-942.
12. Chernova, N.A., M. Roppolo, A.C. Dillon, and M.S. Whittingham, *Layered vanadium and molybdenum oxides: batteries and electrochromics.* Journal of Materials Chemistry, 2009. **19**(17): p. 2526-2552.
13. Moretti, A., F. Maroni, I. Osada, F. Nobili, and S. Passerini, *V_2O_5 Aerogel as a Versatile Cathode Material for Lithium and Sodium Batteries.* ChemElectroChem, 2015. **2**(4): p. 529-537.
14. Petkov, V., P.N. Trikalitis, E.S. Bozin, S.J.L. Billinge, T. Vogt, and M.G. Kanatzidis, *Structure of $V_2O_5{\cdot}nH_2O$ Xerogel Solved by the Atomic Pair Distribution Function Technique.* Journal of the American Chemical Society, 2002. **124**(34): p. 10157-10162.
15. Clites, M. and E. Pomerantseva, *Bilayered vanadium oxides by chemical pre-intercalation of alkali and alkali-earth ions as battery electrodes.* Energy Storage Materials, 2018. **11**: p. 30-37.
16. Clites, M., R. Andris, D.A. Cullen, K.L. More, and E. Pomerantseva, *Improving Electronic Conductivity of Layered Oxides through the Formation of Two-Dimensional Heterointerface for Intercalation Batteries.* ACS Applied Energy Materials, 2020. **3**(4): p. 3835-3844.
17. Liu, X., S. Depaifve, T. Leyssens, S. Hermans, and A. Vlad, *Versatile Synthesis of Vanadium(III, IV, V) Oxides@Reduced Graphene Oxide Nanocomposites and Evaluation of their Lithium and Sodium Storage Performances.* Batteries & Supercaps, 2019. **2**(12): p. 1016-1025.
18. Yao, X., G. Guo, P.-Z. Li, Z.-Z. Luo, Q. Yan, and Y. Zhao, *Scalable Synthesis of Honeycomblike V_2O_5/Carbon Nanotube Networks as Enhanced Cathodes for Lithium-Ion Batteries.* ACS Applied Materials & Interfaces, 2017. **9**(49): p. 42438-42443.
19. Clites, M., B.W. Byles, and E. Pomerantseva, *Effect of aging and hydrothermal treatment on electrochemical performance of chemically pre-intercalated Na-V-O nanowires for Na-ion batteries.* Journal of Materials Chemistry A, 2016. **4**(20): p. 7754-7761.
20. Clites, M., J.L. Hart, M.L. Taheri, and E. Pomerantseva, *Annealing-Assisted Enhancement of Electrochemical Stability of Na-Preintercalated Bilayered Vanadium Oxide Electrodes in Na-Ion Batteries.* ACS Applied Energy Materials, 2020. **3**(1): p. 1063-1075.
21. Clites, M., J.L. Hart, M.L. Taheri, and E. Pomerantseva, *Chemically Preintercalated Bilayered $K_xV_2O_5{\cdot}nH_2O$ Nanobelts as a High-Performing Cathode Material for K-Ion Batteries.* ACS Energy Letters, 2018. **3**(3): p. 562-567.
22. Childres, I., L.A. Jauregui, W. Park, H. Cao, and Y.P. Chen, *Raman spectroscopy of graphene and related materials.* New developments in photon and materials research, 2013. **1**.
23. Xu, B., M.S. Wu, G. Liu, and C.Y. Ouyang, *Understanding the effect of the layer-to-layer distance on Li-intercalated graphite.* Journal of Applied Physics, 2012. **111**(12): p. 124325.
24. Gutić, S., A. Dobrota, N. Gavrilov, M. Baljozovic, I. Pasti, and S. Mentus, *Surface Charge Storage Properties of Selected Graphene Samples in pH-neutral Aqueous Solutions of Alkali Metal Chlorides - Particularities and Universalities.* International journal of electrochemical science, 2016. **11**: p. 8662-8682.
25. Nie, P., C. Min, H.-J. Song, X. Chen, Z. Zhang, and K. Zhao, *Preparation and Tribological Properties of Polyimide/Carboxyl-Functionalized Multi-walled Carbon Nanotube Nanocomposite Films Under Seawater Lubrication.* Tribology Letters, 2015. **58**(1): p. 7.
26. M. Silva, M., D. Ribeiro, E. Cunha, M.F. Proença, R.J. Young, and M.C. Paiva, *A Simple Method for Anchoring Silver and Copper Nanoparticles on Single Wall Carbon Nanotubes.* Nanomaterials, 2019. **9**(10).

27. Deemer, E.M., P.K. Paul, F.S. Manciu, C.E. Botez, D.R. Hodges, Z. Landis, T. Akter, E. Castro, and R.R. Chianelli, *Consequence of oxidation method on graphene oxide produced with different size graphite precursors.* Materials Science and Engineering: B, 2017. **224**: p. 150-157.